ChemComm

COMMUNICATION

View Article Online
View Journal | View Issue

Cite this: *Chem. Commun.*, 2020, **56**, 14645

Received 12th October 2020,
Accepted 29th October 2020

DOI: 10.1039/d0cc06817a

rsc.li/chemcomm

Dynamic chiral cyclohexanohemicucurbit[12]uril†‡

Kamini A. Mishra, [a] Jasper Adamson, [b] Mario Öeren, [c] Sandra Kaabel, [ad] Maria Fomitšenko [a] and Riina Aav *[a]

NMR spectroscopy and DFT modeling studies of chiral cyclohexanohemicucurbit[12]uril indicate that the macrocycle adopts a concave octagonal shape with two distinct conformational flexibilities in solution. Methylene bridge flipping occurs at temperatures above 265 K, while urea monomers rotate at temperatures above 308 K, resulting in the loss of confined space within the macrocycle.

Dynamic molecules capable of adopting distinct shapes in response to external stimuli have driven the development of molecular machines in supramolecular chemistry.[1] Of great importance in this field is the ability to control and direct interactions which can be achieved within the confined spaces of macrocycle cavities. Large macrocycles able to repeatedly undergo significant conformational changes while retaining their molecular integrity have attracted particular interest.[2,3]

Several macrocycles that differ considerably in conformation from their smaller counterparts have been reported. Cyclodextrins (CDs) containing more than 9 glycose units, referred to as large-ring CDs (LR-CDs),[4] can assume a helical folding arrangement, *e.g.*, the 26-membered CD.[5–9] LR-CDs with 14 units have been shown to adopt a conformation that resembles a concave polygon.[10,11] Large pillar[*n*]arenes, where n = 8–10, containing up to 10 monomers in their structures, also adopt concave polygon shapes.[12] Giant calix[*n*]arenes with up to 90 phenolic subunits have been described;[13] however, calix[16]arene is the largest calix[*n*]arene with a known conformation. It has the shape of two superimposed Celtic torcs.[14] The largest reported cucurbituril (CB) contains 15 monomers.[15] CBs with up to 10 monomers display a tubular shape, while homologs with 13 or more monomers are locked into a twisted conformation.[15–18] Hemicucurbiturils (HCs) are single-bridged CB analogues.[19] HC[12], which is formed by the condensation of ethylene urea and formaldehyde and has a highly flexible geometry in solution phase, is the only known 12-membered HC analog.[20] The second-largest known HC is the 8-membered, chiral cyclohexanohemicucurbit[8]uril, **cycHC[8]**,[21–24] which adopts a tubular shape. Despite detection by mass-spectrometry of cycHCs possessing up to 15 members[23,24] and norbornahemicucurbiturils having up to 8 members,[25] only smaller homologs have been isolated, namely **cycHC[6]**s,[21,26–29] bambus[*n*]urils, where n = 4 or 6,[30–35] and biotin[6]urils.[35–38] These smaller 6-membered homologs adopt a relatively rigid conformation with well-defined cavity shapes.

Herein, we describe the synthesis and isolation of the first enantiopure cyclohexanohemicucurbit[12]uril (**cycHC[12]**) and detail its conformational dynamics *via* NMR spectroscopy coupled with density functional theory (DFT) calculations (Fig. 1).

Our findings show that the macrocycle adopts a concave octagon conformation in toluene at low temperatures, while elevated temperatures result in the activation of two dynamic mechanisms: the bridge flip and the monomer flip. Although **cycHC[12]** was previously identified by UV-HPLC in a crude reaction mixture,[23,24] it was not isolated. We have found that subjecting an isolated macrocycle (**cycHC[8]**) or the monomer (cyclohexa-1,2-diylurea) to acidic conditions, in the presence of heptafluorobutyric acid (see S2, ESI‡ for details) leads to the formation of longer oligomers and larger macrocycles. The developed procedure produced **cycHC[12]** with a 1% yield, which permitted elucidation of its shape and conformational dynamics by ^{1}H NMR and DFT. Unfortunately, our attempts to obtain single crystals of **cycHC[12]** from various solvents have been unsuccessful.

[a] *Department of Chemistry and Biotechnology, Tallinn University of Technology, Akadeemia tee 15, 12618 Tallinn, Estonia. E-mail: riina.aav@taltech.ee*
[b] *Chemical Physics Laboratory, National Institute of Chemical Physics and Biophysics, Akadeemia tee 23, 12618 Tallinn, Estonia*
[c] *Optibrium Limited, F5-6 Blenheim House, Denny End Road, Cambridge, CB25 9PB, UK*
[d] *Department of Chemistry, McGill University, 801 Sherbrooke Street West, H3A 0B8, Montreal, Quebec, Canada*

† Dedicated to the memory of late Prof. Hans J. Reich.

‡ Electronic supplementary information (ESI) available: Synthesis, isolation, characterization of **cycHC[12]** by HRMS, 1D and 2D NMR, VT-NMR, conformational dynamics analysis, DFT calculations is described. See DOI: 10.1039/d0cc06817a

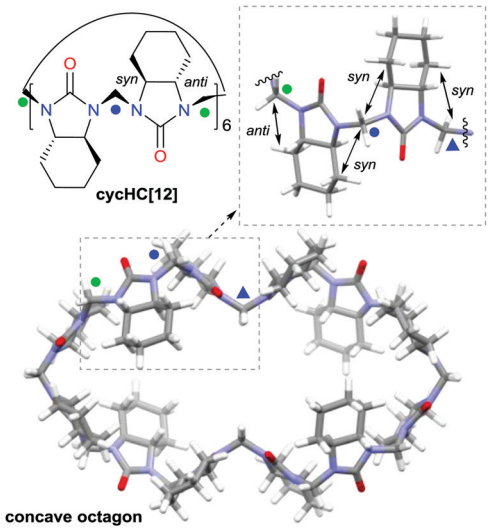

Fig. 1 Chemical structure of **cycHC[12]** and the lowest energy DFT-modelled (BP86/SVP) structure of **cycHC[12]**. Blue and green dots represent *syn*- and *anti*-methylene bridge configurations, respectively. The blue triangle represents the *syn* bridge directed inside the cavity.

Due to the alternating orientations of the cyclohexano-monomers in HCs, the methylene bridges have two possible configurations: *syn* or *anti*. The *syn*- and *anti*-configuration describes the mutual orientation of the bridge and its nearest neighboring cyclohexano carbon skeleton – bridges that are pointed toward the same direction as the cyclohexano skeleton are designated as *syn*. In contrast, those pointed at opposite sides are designated as *anti* (Fig. 1). These distinct bridges, marked by blue and green colored marks (dots or triangles), are shown in Fig. 1–3. Smaller chiral homologs of cycHCs are known to adopt a barrel-shaped conformation with distinct *syn*- or *anti*-oriented bridges in a one-to-one ratio seen in their NMR analysis.[21,27] Thus, a similarly regular 12-gon shape was initially expected for the new chiral **cycHC[12]** macrocycle (Fig. 2, on the right). However, NMR analysis of **cycHC[12]** in toluene at 265 K did not support a highly symmetric regular 12-gon conformation (Fig. 3). The experimental 1D and 2D NMR spectra of **cycHC[12]** instead showed the presence of three non-equal urea groups (α, β, and γ) and four methylene bridges (B1, B2, B3, and B4), indicating the existence of two perpendicular axes of C_2 symmetry

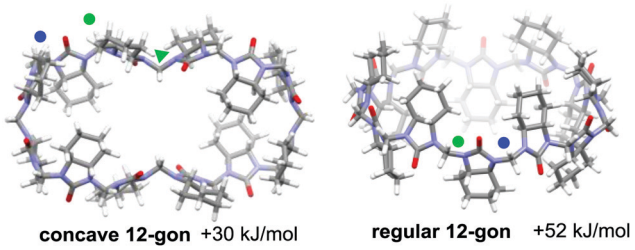

Fig. 2 DFT-modeled structures of **cycHC[12]** (BP86/SVP) higher energy conformers. Blue and green dots represent *syn*- and *anti*-methylene bridge configurations, respectively. The green triangle indicates the *anti*-bridge directed inside the cavity.

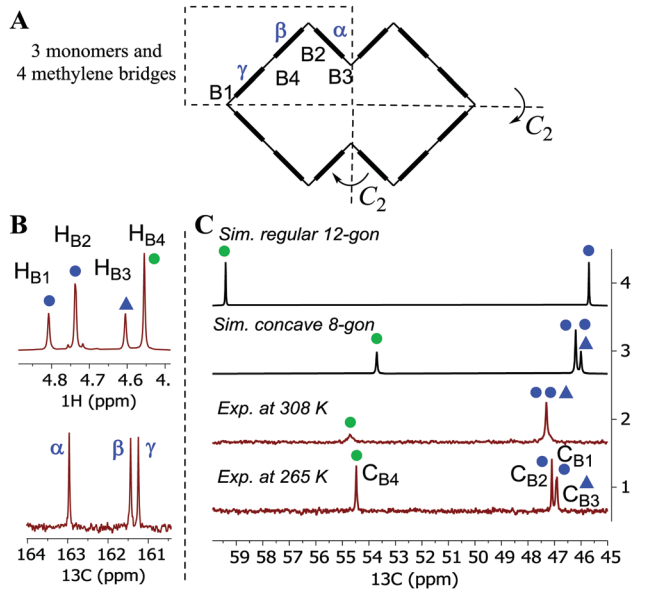

Fig. 3 (A) Symmetry of **cycHC[12]** and the position of symmetry non-related monomers (α, β, γ). (B) NMR spectra of **cycHC[12]** bridge protons H_{B1}–H_{B4} (upper) and carbonyl carbons (lower) in d-toluene. (C) Stacked ^{13}C-NMR spectra of bridge carbons C_{B1}–C_{B4}: (1) experimental at 265 K, (2) experimental at 308 K, (3) simulated for concave octagon, and (4) simulated for regular 12-gon (see simulation details in S20, ESI‡). Blue and green dots designate *syn* (B1 and B2) and *anti* (B4) bridge configurations. The blue triangles represent *syn*-configuration bridges, which are directed inside the cavity (B3).

that divide the structure into four symmetry-related parts (Fig. 3A and B). These structural features, supported by NMR data, suggest a concave polygon conformation, with two methylene bridges flipped towards the center of the cavity (Fig. 1, designated with a triangle).

DFT (BP86/SVP) modeling was used to rationalize the NMR results and investigate the potential **cycHC[12]** conformers. Three initial geometries were selected, the first based on the barrel-like geometry of smaller homologs and the second and third, concave polygons based on the symmetry revealed by the NMR results. The difference between the two concave structures is the configuration of their inwards-pointing methylene groups. The concave octagon conformer has a *syn*-oriented inner bridge marked by the blue triangle (Fig. 1), and the concave 12-gon has an *anti*-oriented inner bridge, marked by the green triangle in (Fig. 2). Of the three optimized structures, the concave octagon conformer is the most prevalent, as it is 52 and 30 kJ mol^{-1} lower in energy than the regular and concave 12-gon conformers (see S18, ESI‡) respectively. Furthermore, the chemical shifts predicted for the concave octagon conformer (Fig. 3C, spectrum 3) are in good agreement with the experimental values (Fig. 3C, spectrum 1), strongly supporting the presence of this **cycHC[12]** conformation at 265 K. The calculated ^{13}C chemical shifts of the regular 12-gon conformation (45.7 and 59.4 ppm) (Fig. 3C, spectrum 4) deviate significantly from the experimental **cycHC[12]** spectra. They more closely resemble those of the barrel-shaped **cycHC[8]** methylene bridges in similar chiral environments (46.88 ppm and 56.04 ppm)

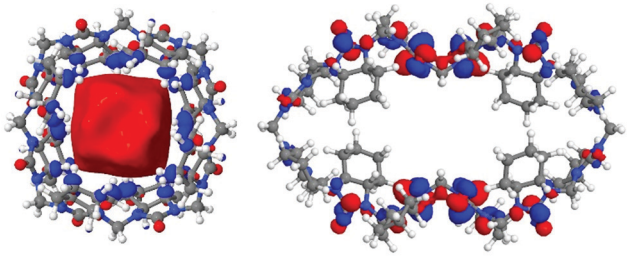

Fig. 4 LUMO of **cycHC[8]** and **cycHC[12]** concave octagons.

(see S20, ESI‡). In the **cycHC[12]** experimental ^{13}C NMR spectra, the *anti*-configuration bridge carbons C_{B4} resonate at a higher frequency (54.48 ppm) than the C_{B3} bridge carbons, which are turned inside the cavity and therefore adopt a *syn* configuration. The latter bridges resonate in a similar range (46.91–47.10 ppm) as the *syn*-oriented bridges C_{B1} and C_{B2} (Fig. 1 and 2). This results from the orientation of C_{B3} into the cavity, causing its electronic environment, and thus its NMR shielding, to resemble the C_{B1} and C_{B2} bridges. In addition, calculations with a higher level of theory, LC-TPSS/aug-pVTZ, were performed to increase the accuracy of the calculated chemical shifts. The addition of long-range corrections made the structures more compact, but the resulting chemical shift values had a greater deviation from the experimental results compared to BP86/SVP (see Table S7, ESI‡). The deviation is due to the compression of **cycHC[12]**, but this is probably not a good representation of the experimental geometry due to the lack of explicit solvent molecules.[39]

Interestingly, the rotation of the two methylene bridges into the cavity induces a conformational change that strongly affects the localization of the frontier orbitals, concentrating the lowest unoccupied molecular orbital (LUMO) on the urea monomers rather than inside the cavity as observed for **cycHC[8]** and all smaller HCs[28,40] (Fig. 4 and S21, ESI‡).

Variable temperature (VT) ^{1}H-NMR spectra show the merging of the H_{B1} signal with the H_{B2} signal and the H_{B3} signal with the H_{B4} signal in pairs between 265 K and 308 K (Fig. 5B, stacked spectra 1 and 6). We suggest this arises from the onset of a dynamic exchange, whereby bridges B1 and B2 and bridges B3 and B4 exchange their magnetic environments in response to the conformational changes of the macrocycle. The merging of the H_{B1} signal with the H_{B2} signal and the H_{B3} signal with the H_{B4} signal both arise from the same conformational changes in the macrocycle. The bridge flip motion can be best explained as a flip of the B3 bridge outwards and the B4 bridge inwards, which simultaneously exchanges the magnetic environments of the B1 and B2 bridge moieties (Fig. 5A). This process reduces the distance between opposing C_{B4} methylene bridges from 18 Å to 7 Å while increasing the distance between C_{B3} bridges. At 265 K, the dynamic exchange is slow, and all bridge environments give separate signals in the ^{1}H NMR spectrum; however, above the coalescence temperature (308 K), the conformations are in fast exchange in the NMR timescale on an 800 MHz spectrometer, resulting in the signals merging (Fig. 5B stacked spectra 6–10).

At temperatures above 308 K, the two resulting proton signals coalesce, indicating an additional mode of dynamic exchange. We hypothesize that this results from the free rotation of the monomers (Fig. 5B stacked spectra 6–10 and Fig. 5C), averaging the magnetic environments of the *syn*- and *anti*-configurations and the inwards and outwards orientations of the bridges. We refer to the second dynamic exchange as the monomer flip. For this process, slow and fast exchange processes are represented by the 308 K and 348 K spectra, respectively (Fig. 5B), and the individual rate constants are available in Table S3 (ESI‡). We undertook line shape analysis of the VT ^{1}H NMR spectra (see Tables S2 and S3 in ESI‡ for fitting details) to derive the activation enthalpy, entropy, and Gibbs free energy values associated with both of the dynamic exchanges (Table 1 and S12, S13, ESI‡). At lower temperatures, the activation Gibbs free energy for the bridge flip is lower than for the monomer flip, which agrees with the monomer flip

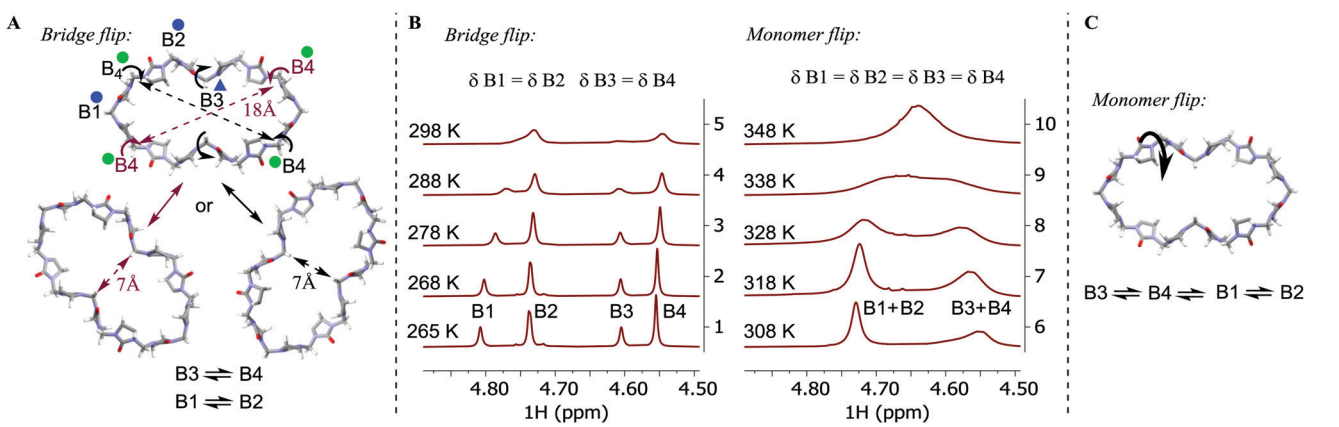

Fig. 5 (A) Illustration of the **cycHC[12]** bridge flip mechanism. Dotted arrows designate bridge moieties that move in relation to the center of the macrocycle. Solid arrows designate conformers in equilibrium. Curved arrows designate the conformational flip. Blue and green dots designate *syn*- and *anti*-bridge configurations, respectively. The triangle represents the bridges directed into the cavity. (B) Evolution of ^{1}H NMR bridge signals at temperatures from 265 K to 348 K showing the (a) methylene bridge flip and the (b) urea monomer flip. (C) Illustration of monomer flip at higher temperatures at which all bridge signals undergo NMR chemical exchange. On structures cyclohexano groups are omitted for clarity.

Table 1 Activation enthalpy, entropy, and Gibbs free energy values for the **cycHC[12]** bridge flip and the monomer flip at 298 K. Notes on the errors in the values are presented in ESI. Values are reported in kJ mol^{-1}

Bridge flip			Monomer flip		
$\Delta H^{\ddagger}$	$T\Delta S^{\ddagger}$	$\Delta G^{\ddagger}$	$\Delta H^{\ddagger}$	$T\Delta S^{\ddagger}$	$\Delta G^{\ddagger}$
38.5 ± 6.1	−25.5 ± 6.3	64.0 ± 8.8	59.9 ± 1.1	−6.6 ± 1.0	66.6 ± 1.5

process having a higher coalescence temperature. It is evident that the bridge flip is more strongly governed by the activation entropy, which we suggest originates from the macrocycle changing its size considerably due to this process.

In conclusion, we have synthesized, isolated, and characterized the conformation of the largest substituted HC homolog to date. **CycHC[12]** contains 12 monomers and resembles a concave octagon at 265 K, as revealed by solution NMR analysis and DFT calculations. VT ^{1}H NMR analysis provides evidence for two dynamic processes at elevated temperatures: a bridge flip and a monomer flip. These dynamic processes have not been observed for the **cycHC[8]** macrocycle due to its small size. We propose that the dynamic characteristics of **cycHC[12]** would allow it to bind larger species and adapt its structure for a guest molecule by taking advantage of the change in cavity diameter of nearly 1 nm.

The authors would like to acknowledge Oliver Paberits and Karin Kreekman for experimental assistance. We also thank the Estonian MER (Grant No. PRG399 and PSG400), the ERDF (CoE 3.2.0101.08-0017, CoE 2014-2020.4.01.15-0013, and CoE TK134), and H2020-FETOPEN (828779 (INITIO)) for financial support.

Conflicts of interest

There are no conflicts of interest to declare.

Notes and references

1 V. Balzani, A. Credi, F. M. Raymo and J. F. Stoddart, *Angew. Chem., Int. Ed.*, 2000, **39**, 3348–3391.
2 L. Cronin, P. A. McGregor, S. Parsons, S. Teat, R. O. Gould, V. A. White, N. J. Long and N. Robertson, *Inorg. Chem.*, 2004, **43**, 8023–8029.
3 X. Chi, G. Yu, L. Shao, J. Chen and F. Huang, *J. Am. Chem. Soc.*, 2016, **138**, 3168–3174.
4 W. Saenger, J. Jacob, K. Gessler, T. Steiner, D. Hoffmann, H. Sanbe, K. Koizumi, S. M. Smith and T. Takaha, *Chem. Rev.*, 1998, **98**, 1787–1802.
5 K. Gessler, I. Usón, T. Takaha, N. Krauss, S. M. Smith, S. Okada, G. M. Sheldrick and W. Saenger, *Proc. Natl. Acad. Sci. U. S. A.*, 1999, **96**, 4246–4251.
6 H. Taira, H. Nagase, T. Endo and H. Ueda, *J. Inclusion Phenom. Macrocyclic Chem.*, 2006, **56**, 23–28.
7 M. G. Gotsev and P. M. Ivanov, *ARKIVOC*, 2007, **13**, 167–189.
8 K. I. Assaf, D. Gabel, W. Zimmermann and W. M. Nau, *Org. Biomol. Chem.*, 2016, **14**, 7702–7706.
9 C. Sonnendecker, S. Thürmann, C. Przybylski, F. D. Zitzmann, N. Heinke, Y. Krauke, K. Monks, A. A. Robitzki, D. Belder and W. Zimmermann, *Angew. Chem., Int. Ed.*, 2019, **58**, 6411–6414.
10 K. Harata, T. Endo, H. Ueda and T. Nagai, *Supramol. Chem.*, 1998, **9**, 143–150.
11 J. Jacob, K. Geßler, D. Hoffmann, H. Sanbe, K. Koizumi, S. M. Smith, T. Takaha and W. Saenger, *Angew. Chem., Int. Ed.*, 1998, **37**, 605–609.
12 X.-B. Hu, Z. Chen, L. Chen, L. Zhang, J.-L. Hou and Z.-T. Li, *Chem. Commun.*, 2012, **48**, 10999–11001.
13 V. Guérineau, M. Rollet, S. Viel, B. Lepoittevin, L. Costa, P. Saint-Aguet, R. Laurent, P. Roger, D. Gigmes, C. Martini and V. Huc, *Nat. Commun.*, 2019, **10**, 1–14.
14 C. Bavoux, R. Baudry, I. Dumazet-Bonnamour, R. Lamartine and M. Perrin, *J. Inclusion Phenom. Macrocyclic Chem.*, 2001, **40**, 221–224.
15 Q. Li, S.-C. Qiu, J. Zhang, K. Chen, Y. Huang, X. Xiao, Y. Zhang, F. Li, Y.-Q. Zhang, S.-F. Xue, Q.-J. Zhu, Z. Tao, L. F. Lindoy and G. Wei, *Org. Lett.*, 2016, **18**, 4020–4023.
16 J. Kim, I.-S. Jung, S.-Y. Kim, E. Lee, J.-K. Kang, S. Sakamoto, K. Yamaguchi and K. Kim, *J. Am. Chem. Soc.*, 2000, **122**, 540–541.
17 W.-H. Huang, S. Liu, P. Y. Zavalij and L. Isaacs, *J. Am. Chem. Soc.*, 2006, **128**, 14744–14745.
18 X.-J. Cheng, L.-L. Liang, K. Chen, N.-N. Ji, X. Xiao, J.-X. Zhang, Y.-Q. Zhang, S.-F. Xue, Q.-J. Zhu, X.-L. Ni and Z. Tao, *Angew. Chem., Int. Ed.*, 2013, **52**, 7252–7255.
19 N. N. Andersen, M. Lisbjerg, K. Eriksen and M. Pittelkow, *Isr. J. Chem.*, 2018, **58**, 435–448.
20 Y. Miyahara, K. Goto, M. Oka and T. Inazu, *Angew. Chem., Int. Ed.*, 2004, **43**, 5019–5022.
21 E. Prigorchenko, M. Oeren, S. Kaabel, M. Fomitsenko, I. Reile, I. Jarving, T. Tamm, F. Topic, K. Rissanen and R. Aav, *Chem. Commun.*, 2015, **51**, 10921–10924.
22 S. Kaabel, J. Adamson, F. Topić, A. Kiesilä, E. Kalenius, M. Öeren, M. Reimund, E. Prigorchenko, A. Lõokene, H. J. Reich, K. Rissanen and R. Aav, *Chem. Sci.*, 2017, **8**, 2184–2190.
23 M. Fomitšenko, E. Shmatova, M. Öeren, I. Järving and R. Aav, *Supramol. Chem.*, 2014, **26**, 698–703.
24 S. Kaabel, R. S. Stein, M. Fomitšenko, I. Järving, T. Friščić and R. Aav, *Angew. Chem., Int. Ed.*, 2019, **58**, 6230–6234.
25 T. Fiala and V. Sindelar, *Synlett*, 2013, **24**, 2443–2445.
26 Y. Li, L. Li, Y. Zhu, X. Meng and A. Wu, *Cryst. Growth Des.*, 2009, **9**, 4255–4257.
27 R. Aav, E. Shmatova, I. Reile, M. Borissova, F. Topić and K. Rissanen, *Org. Lett.*, 2013, **15**, 3786–3789.
28 M. Öeren, E. Shmatova, T. Tamm and R. Aav, *Phys. Chem. Chem. Phys.*, 2014, **16**, 19198–19205.
29 E. Prigorchenko, S. Kaabel, T. Narva, A. Baškir, M. Fomitšenko, J. Adamson, I. Järving, K. Rissanen, T. Tamm and R. Aav, *Chem. Commun.*, 2019, **55**, 9307–9310.
30 O. Reany, A. Mohite and E. Keinan, *Isr. J. Chem.*, 2018, **58**, 449–460.
31 T. Lizal and V. Sindelar, *Isr. J. Chem.*, 2018, **58**, 326–333.
32 J. Svec, M. Necas and V. Sindelar, *Angew. Chem., Int. Ed.*, 2010, **49**, 2378–2381.
33 M. A. Yawer, V. Havel and V. Sindelar, *Angew. Chem., Int. Ed.*, 2015, **54**, 276–279.
34 V. Havel, M. Babiak and V. Sindelar, *Chem. – Eur. J.*, 2017, **23**, 8963–8968.
35 V. Havel, J. Svec, M. Wimmerova, M. Dusek, M. Pojarova and V. Sindelar, *Org. Lett.*, 2011, **13**, 4000–4003.
36 M. Lisbjerg, B. M. Jessen, B. Rasmussen, B. E. Nielsen, A. Ø. Madsen and M. Pittelkow, *Chem. Sci.*, 2014, **5**, 2647–2650.
37 M. Lisbjerg, B. E. Nielsen, B. O. Milhøj, S. P. A. Sauer and M. Pittelkow, *Org. Biomol. Chem.*, 2015, **13**, 369–373.
38 M. Lisbjerg, H. Valkenier, B. M. Jessen, H. Al-Kerdi, A. P. Davis and M. Pittelkow, *J. Am. Chem. Soc.*, 2015, **137**, 4948–4951.
39 M. A. Iron, *J. Chem. Theory Comput.*, 2017, **13**, 5798–5819.
40 T. F. G. G. Cova, S. C. C. Nunes, A. J. M. Valente, T. M. V. D. Pinho e Melo and A. A. C. C. Pais, *J. Mol. Liq.*, 2017, **242**, 640–652.

